Thermal, optical and electrical properties of MnO$_2$-doped mixed sodium potassium phosphate glasses

M. Jerroudi[1] · L. Bih[1,2] · S. Yousfi[2] · L. Bejjit[3] · M. Haddad[3] · B. Manoun[4,5] · P. Lazor[6]

Abstract

Glasses in the system $(1-x)(0.5\text{NaPO}_3–0.5\text{KPO}_3)–x\text{MnO}_2$, with $0 \leq x \leq 50$ mol%, have been prepared using a melt-quench route. The glasses exhibit a yellow to dark color with the increase in manganese content owing to the presence of Mn^{2+} and Mn^{3+} ions in the network. The amorphous state of the glasses is evidenced by the X-ray diffraction. In order to get an insight into the physical and structural aspects of these vitreous materials, we have determined some of their parameters such as density, molar volume and glass transition temperature. From differential thermal analysis scan on heating, we evaluated the glass transition temperature (T_g) of each glass, which corresponds to the phase transition temperature from solid to viscous liquid. The density (ρ) as a structural index is found to increase while the corresponding molar volume decreases with MnO$_2$ content. The structural approach of the studied glasses is evaluated by infrared (IR) and electron paramagnetic resonance (EPR) spectroscopies. IR technique allowed us to identify the coexisting bond vibration modes in the glass network, and it has shown that many structural phosphates units coexist, mainly pyrophosphate and metaphosphate structural groups. EPR experiments have shown the presence of Mn^{2+} centers in the glasses. The UV–Visible absorption is utilized to estimate the values of the optical band gap (E_g) and Urbach energy (ΔE). The optical band gap energy is determined from both the absorption spectrum fitting (ASF) and Tauc's methods. These optical parameters are composition dependence. The dc conductivity of the glasses is determined in the temperature range from 303 to 473 K. It decreases with increasing manganese content. It is thermally activated and followed an Arrhenius behavior. The crystallization of glasses is realized by submitting them to heat treatments, and the crystallized phases are identified by XRD analysis. The crystallization kinetic was studied under non-isothermal conditions. The activation energy (E_c) and the Avrami parameter (n) were determined.

Keywords Phosphate · Glasses · Crystallization · Structure · Optical · Conductivity

Introduction

In recent years, the number of studies of phosphate glasses has raised since they possess many unique properties. These materials can be elaborated at low melting temperatures compared to borate and silicate glasses. They are used in various applications such as the manufacturing of glass polymer composites, glass to metal seals [1] and conductor materials [2]. In addition, the combination of phosphate with many transition metal ions (TMI) forms glasses with specific electrical, optical and magnetic properties [3, 4].

One of the main interesting transition metal oxides inserted in glasses is manganese MnO. It is used in the coloring of glasses. Manganese showed various valence states, and its coordination varies with the glass former nature. It is found that the oxidation state of manganese in the glasses depends on the chemical composition and the field strength

✉ L. Bih
bihlahcen@yahoo.fr

1 Equipe de Physico-chimie de la Matière Condensée, PCMC, Faculté des Sciences de Meknès, Meknes, Morocco

2 Laboratoire des Sciences et Métiers de l'Ingénieur (LSMI), Département matériaux et procédés, ENSAM Meknès, Université Moulay Ismail, Meknes, Morocco

3 Laboratoire de Spectrométrie, des Matériaux et Archéomatériaux (LASMAR), Faculté des Sciences de Meknès, Université Moulay Ismail, Meknes, Morocco

4 FST, Rayonnement-Matière et Instrumentation, S3M, Hassan First University of Settat, 26000 Settat, Morocco

5 Materials Science and Nano-engineering Department, University Mohammed VI Polytechnic, Ben Guerir, Morocco

6 Department of Earth Sciences, Uppsala University, 752 36 Uppsala, Sweden

of the modifiers and the glass formers [3]. For instance, in borate glasses, manganese exists in the form of Mn^{2+} and Mn^{3+} in octahedral sites [5]. In silicate and germinate glasses, it is in the form of Mn^{2+} with tetrahedral and octahedral environments [6]. It is also indicated that Mn^{2+} or Mn^{3+} cations may be present as a mixture in the glasses. In phosphate $xMnO–40P_2O_5–(60−x)ZnO$ glasses [4], it is reported that manganese exists mainly as Mn^{2+} ions and it is found that MnO behaved as a structural modifier oxide. In the system $(50−x/2)Na_2O–xMnO–(50−x/2)P_2O_5$ [7], the substitution of Na_2O and P_2O_5 by MnO increased the values of the density and the glass transition temperature. The increase in the physical parameters is attributed to the formation of P–O–Mn bonds that crosslink the glass lattice. The effect of the replacement of potassium with manganese within the glasses $(50−x)K_2O–xMnO–50P_2O_5$ has been studied [8]. It is found that MnO played a modifier role and depolymerized the phosphate network. The covalent P–O–Mn bonds are formed as in the case of sodium-based phosphate vitreous materials. The investigation of valency state of manganese in the above sodium and potassium phosphate materials is not investigated.

Recently, we have developed thermal stable phosphate $(1−x)(NaPO_3–KPO_3)–xZnO$ glasses [9]. These materials are characterized by the coexistence of mixed alkaline elements, known to reduce the melting temperature of the glasses, and ZnO which enhances some of their physical and chemical properties. According to our knowledge, there is no work on the effect of the substitution of both sodium and potassium by manganese in phosphate glasses. So, we have focused our interest to study the combination of the positive influence of manganese to increase the chemical resistance and the mixed sodium and potassium effect to produce low melting glasses. Manganese is always introduced in the glasses as MnO oxide. In this study, we use MnO_2 as a source of this element.

According to our investigation, few data were reported on the physical, optical and electrical properties of manganese phosphate glass system containing both sodium and potassium oxide [9, 10]. So, the research purpose of this work is the development of phosphate glasses that have the ability to be formed at low melting temperature. To achieve this objective, we consider the glasses belonging to the system $(1−x)(0.5NaPO_3–0.5KPO_3)–xMnO_2$ where the ratio (Na_2O/ K_2O) is kept constant. The particularity of these glasses is the combination of the positive effect of manganese oxide (MnO_2) to improve the chemical durability and the mix of two alkali oxide (Na_2O and K_2O) which leads to lowering the melting temperature. The thermal properties of these glasses are studied by differential thermal analysis (DTA) technique. Infrared spectroscopy is performed to identify different units developed within the amorphous network. While UV–visible absorption has highlighted the presence

of Mn^{2+} and Mn^{3+} in the glassy network, EPR has identified the presence of Mn^{2+} centers. The glasses under study contain both manganese in +2 and +3 valence states. The effect of manganese oxide on electrical properties is investigated. It is found that dc conductivity decreases with increasing manganese content. The crystallization kinetic is performed using DTA thermal analysis, and the crystalized phases were identified by XRD diffraction.

Experimental procedures

Glass preparation

The glass samples having the general formula $(1−x)(0.5NaP O_3–0.5KPO_3)–xMnO_2$ with $0 \leq x \leq 50$ mol% have been prepared by weighing suitable amount of the starting reagents $(NH_4)_2HPO_4$, Na_2CO_3, K_2CO_3, and MnO_2. The samples are mixed together by grinding the mixture repeatedly to obtain a fine powder. This mixture is put in alumina crucible and fired at 300 °C in an electric furnace in order to remove ammonia and humidity from the phosphate precursor. Then, the temperature is gradually raised to 600 °C to decarbonate and decompose the sodium and potassium carbonates. Finally, the oven temperature is increased to 900 °C to reach the molten state. The melt is finally quenched to room temperature under air. The vitreous samples are annealed for 4 h at about 50 °C under the glass transition temperature to relieve residual internal stress and slowly cooled at room temperature. The glasses are then stored under vacuum in a desiccator to prevent possible moisture. They have been labeled as NKPMx, where x indicates the manganese concentration.

Characterization of the glasses

X-ray diffraction (XRD) is used to confirm the amorphousness of each sample by using an X-ray powder diffraction instrument (LabX XRD-6100) equipped with a CuK_α X-ray source and a Ni filter ($\lambda_{Cu} = 1.5406$ Å). The XRD diffractograms were recorded at room temperature (RT) in 2θ range 10°–70° with a scan rate of 0.02° min^{-1}.

Density measurements of the glass sample are carried out using a densimeter (H 300S) and water as a fluid medium. The density (or specific volume) resolution is estimated at around ± 0.001 g cm^{-3}. For each of the samples, the density is measured using the following relationship:

$$\rho = W_{air}/ W_{air} − W_{water} \tag{1}$$

where (W_{air}) and (W_{water}) each represent the sample's weights in air and water, respectively. The molar volume of the

samples (V_m) is calculated from the density and the glass molar weight by the expression below:

$$V_m = \sum_i x_i M_i / \rho \qquad (2)$$

where (M_i) is the molecular weight of an oxide component (i) and (x_i) is its mole fraction.

The differential thermal analysis (DTA) was carried out in the temperature range 100–600 °C using a SHIMADZU DTA-60 analyzer. DTA runs are realized on ground glass of about 50 mg and heated in alumina crucible at different heating rates from 5 to 20 °C min⁻¹, and the temperature measurement error is about ± 2. The reference for measurement is an alumina crucible. The crystallization process is realized by submitting the samples to heat treatments between 510 and 600 °C depending on the composition.

To identify the structural units in the structure of the glasses, the infrared absorption spectra of the glasses are carried out at room temperature in the wavenumber range 1400–400 cm⁻¹ using a TENSOR27 spectrometer. The analysis is made on the sample pellets in KBr matrix (1:300 mg).

The identification of the crystalline phases in the glass–ceramics is performed by XRD analysis. The crystallization process is realized by submitting the glass samples to heat treatments at the characteristics temperature (T_c) for 16 h.

For the optical characterization of the glasses, a UV–Vis spectrometer Jascov-570 using a barium sulfate (BaSO₄) plate on which finely ground glass sample is coated is used to estimate the optical band gap and the Urbach energy over the spectral ranges 200–800 nm at room temperature.

The optical band gap energy for the present samples was determined by employing the Tauc's plots and the ASF method. In the ASF method, the determination of the optical band gap energy depends only on the sample absorbance. The absorption coefficient $\alpha(v)$ near the edge is calculated according to the relation [11]:

$$\alpha(v) = (2.303/d) A(v) \qquad (3)$$

where "A" is the absorbance and "d" is the thickness of the sample (in centimeters).

Generally, for the amorphous and vitreous materials, Davis and Mott [11] described the optical absorption $\alpha(v)$ above the exponential tail by the following power-law expression:

$$\alpha h v = \alpha (h v - E_g)^n \qquad (4)$$

where "n" is an index that can have different values: 2, 3, 1/2 and 1/3 corresponding to indirect allowed, indirect forbidden, direct allowed and direct forbidden transitions; Davis and Mott proposed that most amorphous semiconductors have allowed direct transitions and (n) is 2. "B" is a constant

called band tailing parameter, "E_g" is the optical band gap energy, and $h v$ is the incident photon energy.

The gap energy is also determined by the ASF method by rewriting Eq. (3) as a function of the wavelength (λ) [12]:

$$A(\lambda) = D\lambda \left(l/\lambda - l/\lambda_g \right)^m \qquad (5)$$

where "$\alpha(\lambda)$" is the absorption coefficient, "λ_g" is the wavelength corresponding to the optical gap, $D = [B(hc)^{m-1}d/2.303]$, d is the sample thickness and A is the corresponding absorbance.

In order to estimate the disorder degree of the glasses and the effect of manganese on it, we have determined the Urbach energy according to the equation [13]:

$$\alpha(v) = B \exp(h v / \Delta E) \qquad (6)$$

where ΔE is the Urbach energy and B is a constant.

To identify paramagnetic centers in the glasses, the EPR spectra are conducted at room temperature by using an electron paramagnetic resonance (EPR) spectrometer (Bruker ER 200D) operating in the X-band frequencies (9.5 GHz) with a modulation frequency of 100 kHz. A powdered glass specimen of 100 mg was taken in a quartz tube for measurements. Polycrystalline 2,2 diphenyl-1-picrylhydrazyl (DPPH) with g value of 2.0036 is used as a standard field marker.

The electric measurement of the glasses is performed as a function of both temperature (303–473 K) and frequency (10 Hz–1 MHz) using Modulab MTS Solartron impedance analyzer driven by a microcomputer and connected to the Probostat cell holder system.

Results and discussion

Glassy formation and XRD analysis

The glasses we investigate in this work have the compositions $(1-x)(0.5\text{NaPO}_3 – 0.5\text{KPO}_3) – x\text{MnO}_2$, and their positions in the diagram NaPO₃–KPO₃–MnO₂ are shown in Fig. 1. The homogeneous samples could be elaborated up to 50 mol% MnO₂. The homogeneity is assumed regarding the transparency and the absence of any visual defects. The amorphous structural nature of them is checked by X-ray diffraction analysis. XRD patterns for different samples (Fig. 2) show only one broad halo at low angles. Indeed, there is no peak, characteristic of crystalline materials, which attests the amorphous state of these glassy samples. It is worth noting that the position of the broad peak is shifted toward lower angle for the first 10 mol% Mn²⁺ substitution for Na⁺ and K⁺ (NKPM10). This could be due to topologic ordering of the ions caused by atomic rearrangement. This indicates that the incorporation of manganese up to 10 mol% affords an
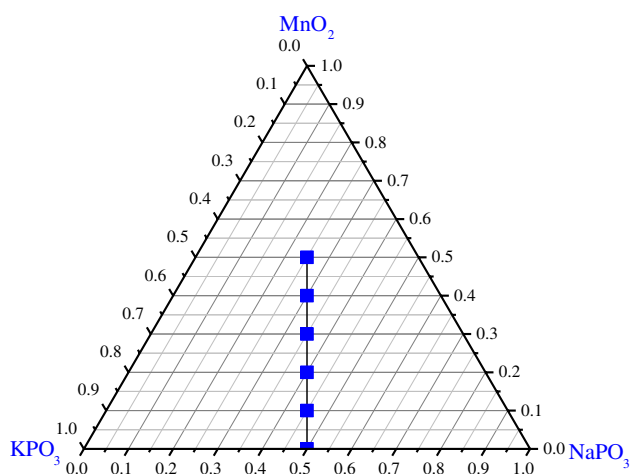
Fig. 1 Locations of the glasses inside the diagram $NaPO_3$–KPO_3 MnO_2

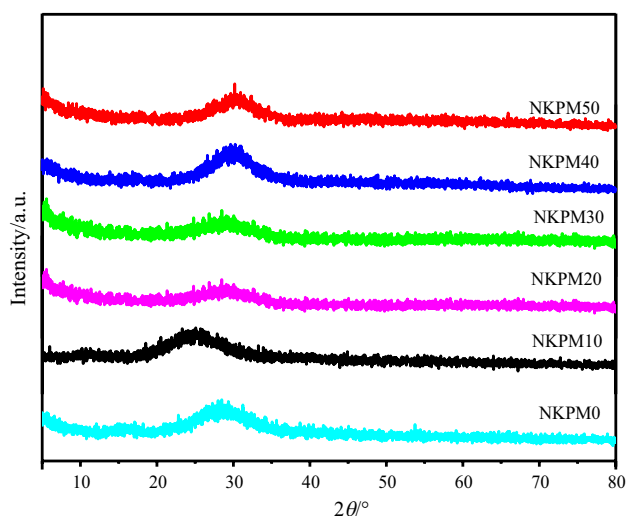**Fig. 2** X-ray patterns of the $(1-x)$ $(0.5NaPO_3-0.5KPO_3)-xMnO_2$ glasses

expansion of the phosphate glassy network due to topologic ordering of the ions caused by atomic rearrangement in the amorphous lattice. On the other hand, for further addition of manganese, the XRD halo position shifts slightly toward

larger angle, suggesting that manganese contributes to the reticulation of the glassy network.

Density and molar volume

The density is an important intrinsic property that gives a good idea about the compactness of materials, and it can provide information on the short-range structure of vitreous materials. It is well known that it is not easy to conclude exactly the structure and the atomic arrangements in glasses without using different techniques; however, the density data remain to be a fundamental test for a short-range order model [14]. The density (ρ), molar volume (V_m) and the oxygen packing density (OPD) for the present glass system are collected in Table 1. Density of the studied glasses increases with the MnO_2 content and passes from 2.44 to 2.89, while molar volume decreases from 45.11 to 34.93 (cm^3 mol^{-1}) as shown in Fig. 3. The glass density increase can be understood from the fact that the mass weight of manganese oxide is larger than that of alkali phosphate oxides. Moreover, this increase can be due to the change of the bond linkage nature in the structure. For instance, the substitution of alkali ions by manganese causes the replacement of the ionic linkages (PO^-, A^+) (A = Na, K) issued from the matrix ($NaPO_3$–KPO_3) by the covalent bonds P–O–Mn. The presence of these latter bond type enhances the reticulation of the glass network. Oxygen packing density (OPD) values of the studied glasses are found to increase from 68.52 to 75.31 mol l^{-1} with MnO_2 content. This behavior can be explained by the increase in number of oxygen atoms per unit composition, which results in high connectivity and reticulation in the glass network. Therefore, it can be assumed that the introduction of manganese in the glasses reticulates the phosphate groups and renders the glassy structure denser at higher MnO_2 content. A similar reticulation effect of manganese is reported in other phosphate glasses [7, 8]. In parallel, the molar volume decreases from 45.11 for NKPM0 ($x=0$) to 34.93 cm^3 mol^{-1} for NKPM50 ($x=50$) mol% of MnO_2 content. This decrease could be associated with the decrease in the interstitial space between the polyhedra and/or the size of the porous space which is induced by the reticulation effect of manganese ions.

Table 1 Some physical properties of the $(1-x)$ $(0.5NaPO_3-0.5KPO_3)-xMnO_2$ $(0 \leq x \leq 50$ mol%) glasses

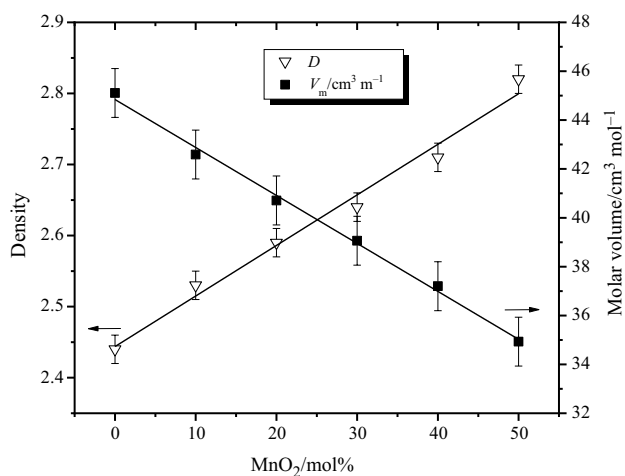| Sample code	x/mol%	O/P ratio	Density	OPD	V_m/cm^3 mol^{-1}	T_g/°C	g-factor
NKPM0	0	3	2.44	66.52	45.11	245	–
NKPM10	10	3.11	2.53	68.52	42.59	260	2.02
NKPM20	20	3.25	2.59	69.62	40.71	284	2.01
NKPM30	30	3.42	2.64	70.34	39.06	303	2.02
NKPM40	40	3.66	2.71	71.48	37.20	326	2.02
NKPM50	50	4	2.82	73.48	34.93	362	2.01

Fig. 3 Composition dependence of the density and the molar volume

DTA study

The DTA curves of the glasses recorded at a constant heating rate of 20 °C min^{-1} are shown in Fig. 4. The glass transition temperature (T_g) of each glass corresponds to line deviation in the curve. The characteristic temperatures are determined and gathered in Table 1. From the analysis of these data, it is observed that the replacement of a part of NaPO$_3$–KPO$_3$ by MnO$_2$ leads to an increase in T_g from 245 °C (NKPM0) to 362 °C (NKPM50), and about one hundred degrees difference exists between the manganese-free glass and the high-manganese one. The variation in the glass transition
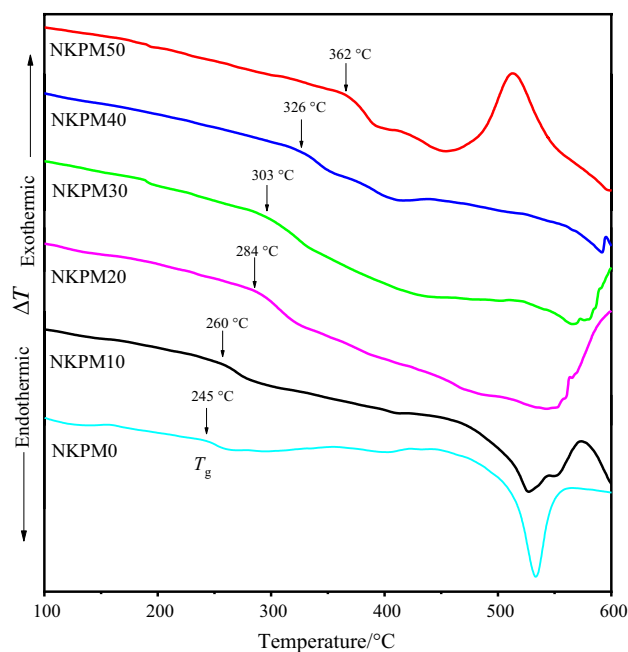
temperature as a function of the MnO$_2$ is illustrated in Fig. 5. The composition dependence of the T_g is associated with the nature of the chemical bonds present in the glasses. It is well known that the glass transition temperature is sensitive to the glass structure [15]. It depends on the bonding force, the degree of crosslink density and the tightness/closeness of the network. An increase in each of these parameters contributes to the increase in T_g. Firstly, the increase in T_g with increasing manganese content is due to the formation of the more covalent P–O–Mn bonds in the vitreous lattice at the expense of the more ionic P–O–A (A = K, Na) links. The larger covalent character of P–O–Mn bond than that of the P–O–A link results from the fact that the electrical field strength is larger for Mn^{2+} than for K$^+$ and Na$^+$. The formation of covalent bonds was observed in other phosphate glasses containing Mn^{2+}, Cd^{2+} and Pb^{2+} [16]. Secondly, the parameter that determines the density of the oxygen polyhedra in the glass (OPD) is represented in Fig. 5. It shows an increasing behavior with manganese oxide. It can be deduced then that packing oxygen density (OPD) contributes also the increase in T_g. Lastly, the increase in T_g could be due also to the increase in the closeness packing of the network while adding the manganese oxide. Indeed, the chemical formula of the glasses (1 − x)(0.5NaPO$_3$–0.5KPO$_3$)–xMnO$_2$ (x = 0–50 mol%) can be described by two sub-systems (0.5 − x/2)NaPO$_3$–xMnO$_2$ and (0.5 − x/2)KPO$_3$–xMnO$_2$. It is worth noting that the introduction of manganese instead of alkali oxides in the structure corresponds to: (1) the increase in the reticulation of the glassy framework by manganese and (2) the reduction in the depolymerization effect caused by K$_2$O and Na$_2$O modifier oxides. Thus, the reticulation effect of manganese corroborates the increase in T_g when the MnO$_2$ content increases in the glasses.

Fig. 4 DTA curves of the studied glasses
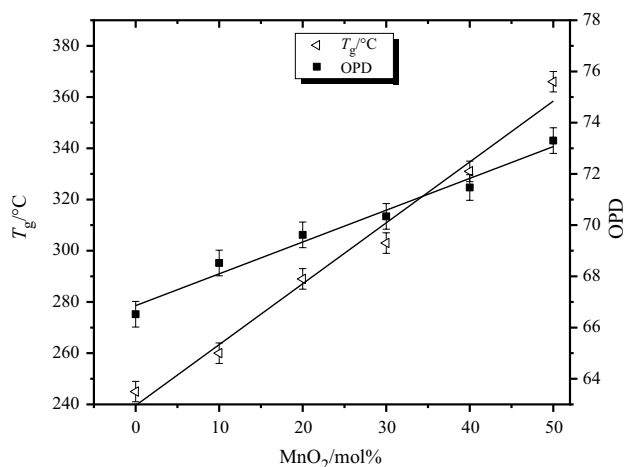

Fig. 5 Glass transition temperature (T_g) and OPD versus the composition for the glasses (line is drawn as a guide to the eye)
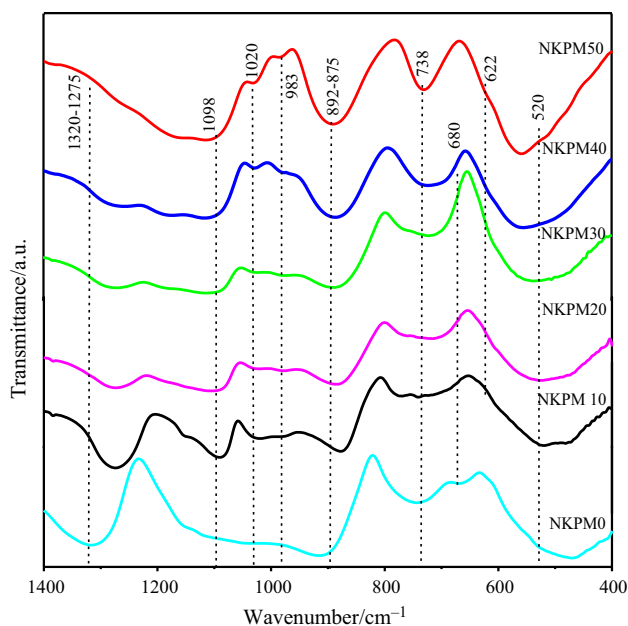
Fig. 6 Infrared spectra of the $(1-x)(0.5NaPO_3–0.5KPO_3)–xMnO_2$ glasses

Table 2 Positions of the infrared bands and their assignments

Position/cm^{-1}	Assignments
1275	ν_{as} (P=O), Q^3 + ν_{as} (PO$_2$), Q^2
1098–1090	ν_{as} (PO$_3$), Q^1
1020	ν_s (PO$_3$), Q^1
983–977	ν_{as} (PO$_4$), Q^0
892–875	ν_{as} (P–O–P)
738	ν_s (P–O–P), Q^1
708	ν_s (P–O–P), Q^2
622	Mn–O, MnO$_6$
510–560	δ(PO$_4$)

Infrared spectroscopy

Infrared spectroscopy is used to get information about the glass structure via the identification of different structural groups. The FTIR spectra of the glassy samples are shown in Fig. 6. The infrared band positions and their assignments are listed in Table 2. The assignment of the bands is recognized according to the literature data of similar glasses [7–9]. The band near 1310–1275 cm^{-1} is related to the asymmetric stretching vibration ν_{as}(PO$_2^-$) in metaphosphate (Q^2) structural units and/or the asymmetric stretching of the doubly bonded oxygen vibration ν_{as}(P=O). The band in 1098 cm^{-1} is ascribed to the asymmetric vibration mode of the chain end group ν_{as}(PO$_3^{2-}$), characteristic of pyrophosphate unit Q^1. The band around

1020 cm^{-1} appearing with the increase in manganese content is due to the symmetric stretching ν_s(PO$_3^{2-}$) of the Q^1 end group. The band around 983 cm^{-1} is associated with the asymmetric vibration ν_{as}(PO$_4^{3-}$) of the monophosphate Q^0 structural unit. The asymmetric and symmetric vibration modes of P–O–P bonds in Q^1 units, ν_{as}(P–O–P) and ν_s(P–O–P), are ascribed to bands around 875–892 cm^{-1} and 738 cm^{-1}, respectively. The band at about 680 cm^{-1} is attributed to the symmetric stretching vibration of ν_s(P–O–P) in Q^2 structural groups. With further increase in manganese content in the network, a shoulder near 622 cm^{-1} appears in the spectra of the glasses containing more than 20 mol%. This feature is due to the vibration mode of the Mn–O bond in the polyhedra MnO$_6$ structural unit [17]. The band lying under 520 cm^{-1} is ascribed to the deformation mode of (PO$_4$) groups.

From the analysis of Fig. 6, it is obvious that the introduction of MnO$_2$ in the network has induced some structural modifications which are manifested by the IR shape change when the content of manganese is higher than 20 mol%. These changes are linked to the formation of pyrophosphate and orthophosphate structural units. It is accepted that the addition of modifier oxides to the vitreous-P$_2$O$_5$ glass former leads to depolymerize its glassy structure. The depolymerization of phosphate network can be described by the pseudo reaction $2Q^n + R_2O \rightarrow Q^{n-1}$ [18]. By assuming that MnO$_2$ in the glasses behaves as a modifier oxide, the increase in its content results in the broken of metaphosphate chains and the formation of short phosphate groups such as (P$_2$O$_7$)$^{4-}$ and (PO$_4$)$^{3-}$. The above assumption is confirmed by the appearance of a band at 1020 cm^{-1}, characteristic of pyrophosphate unit (Q^1) and a small band around 983 cm^{-1} relative to orthophosphate units (Q^0). The formation of these depolymerized phosphate units is in agreement with the increase in the O/P ratio with increasing manganese contents. Moreover, the mode relative to ν_{as}(P–O–P) displaces toward the high wavenumbers, from near 877 to 892 cm^{-1}, with increasing MnO$_2$ content. This result can be attributed to the increase in the covalent character of the P–O–P bonds, telling that these bonds are enhanced when Na$^+$ and K$^+$ are replaced by Mn^{2+}. It is worth noting also that the intensity of the band relative to ν_{as}(P=O) decreases. The inference is some P=O bonds are converted to P–O–Mn with the incorporation of MnO$_2$ into the glassy network. From the IR investigation, we can deduce that MnO$_2$ depolymerizes the glass framework, plays a modifier structural role and exists in the glassy matrix as (MnO$_6$) groups [19]. According to this modifier effect, one can expect the decrease in the glass transition temperature T_g with increasing MnO$_2$ content. However, contrarily to what would be expected, T_g increases (Fig. 5) owing to the reticulation effect of this manganese oxide.

Optical properties

The UV–visible spectra for glassy system $(1-x)(0.5\text{NaP}O_3-0.5\text{KPO}_3)-x\text{MnO}_2$, $x = 0–50$ mol%, in the range 200–800 nm are presented in Fig. 7. The spectrum of Mn-free glass contains one band at high energy as usual for amorphous materials. The impurities such as Fe^{3+} ions present in the vitreous composition could also contribute to this absorption band [20]. However, that of Mn-doped glasses shows two broad bands. These features are associated with the charge transfer and the d–d transitions in the Mn species. The edge absorption around 200–350 nm may be due to the transfer charge (TC) between the oxygen $2p$ and the $3d$ orbital of manganese ion. The second broad band at about 420–600 nm in the absorption spectra is due to d–d transitions of Mn^{2+} (d^5) and Mn^{3+} (d^4) ions in octahedral sites according to the fact that the absorption band of Mn^{2+} ion appeared above 420 nm and that of Mn^{3+} between 380 and 600 nm [21]. Since the d–d transitions of Mn^{3+} and Mn^{2+} are spin allowed and spin forbidden, respectively, one can suggest that the absorption spectra are more sensitive to the variation in the Mn^{3+} content than that of Mn^{2+}. It is observed that the d–d transitions band shifts slowly to longer wavelengths while its intensity increases when the concentration of MnO_2 goes up. This fact could indicate that the amount of Mn^{3+} ion is increased in high-manganese glasses. However, this content would be small in comparison with Mn^{2+} content since in Mn_2O_3-doped phosphate glasses [22] where Mn is added to the glasses as a trivalent state was under 3 mol%.
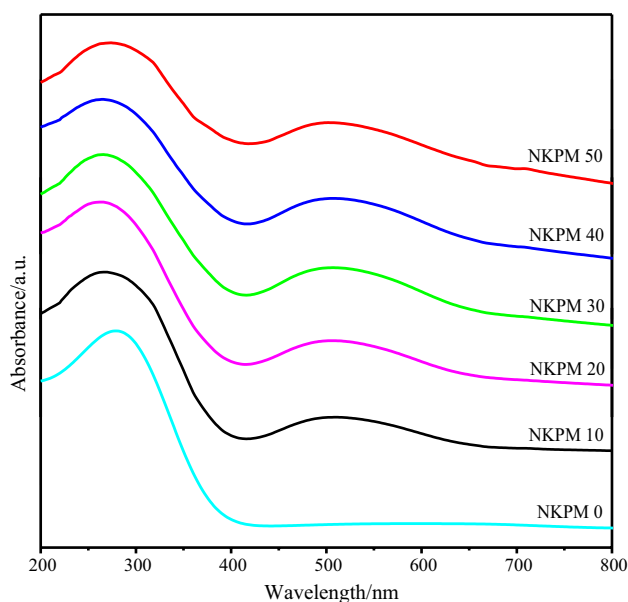
Figure 8 depicts the Tauc plots for the glassy samples. From the variation in $(\alpha h\upsilon)^{1/2}$ versus photon energy ($h\upsilon$), one can determine the optical band gap for the samples. According to this graph, the optical band gap energy (E_g) can be determined by the extrapolating of the linear region of the curve to the x-axis at $\alpha = 0$ (Eq. 3). This parameter (E_g) can be also determined by the other method called ASF method (Fig. 9) using (Eq. 4). It is observed that as the manganese content increases, the optical band gap decreases (Fig. 10). This behavior was observed in several glasses systems, and it is mostly attributed to the change in the glass network and formation of non-bridging oxygen bonds [23]. Thus, the observed decrease in E_g indicates that the introduction of MnO_2 in the glass creates more non-bridging oxygen atoms, in agreement with the infrared results which indicate that MnO_2 played a modifier structural role. It seems that manganese ions occupy modifier sites in the network as alkali ions do. The substitution of alkali by manganese ions in glasses is realized in such a way that manganese ions locate in the modifier sites left by the alkali ions (Na^+ and K^+). In other words, manganese ions play the modifier structural role as alkali ions. The higher the content of manganese is, the higher the number of non-bridging oxygen in the glasses is. Therefore, the increase in the manganese ratio in the glass induces the decrease in the band gap energy.

The Urbach's plots $(\ln(\alpha) = f(h\upsilon))$ are shown in Fig. 11. The Urbach energy gives an estimation of the order or disorder effects in amorphous or crystalline systems. The obtained values of ΔE for the present glass system lie between 0.34 and 0.54 eV and are reported in Table 3. These values have the same order to that reported for oxide glasses in the literature [24]. The composition dependence of the Urbach energy shows that it increases with increasing MnO_2
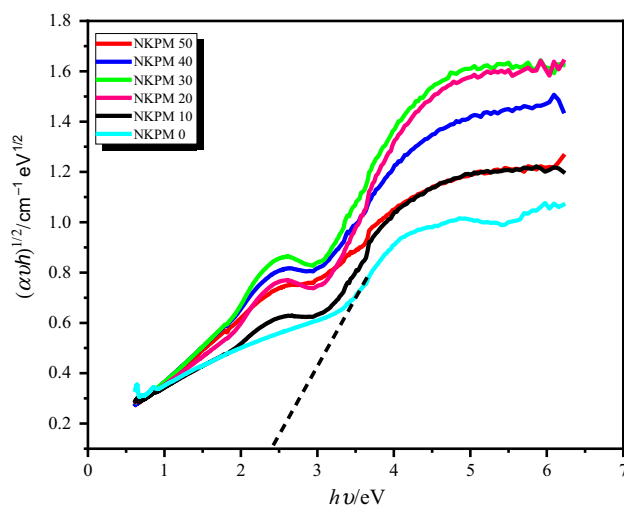

Fig. 7 Optical absorption spectra in the range 200–800 nm for the studied glasses

Fig. 8 Variation in $(\alpha h\upsilon)^{1/2}$ as a function of photon energy ($h\upsilon$) for the studied glasses (Tauc's method)
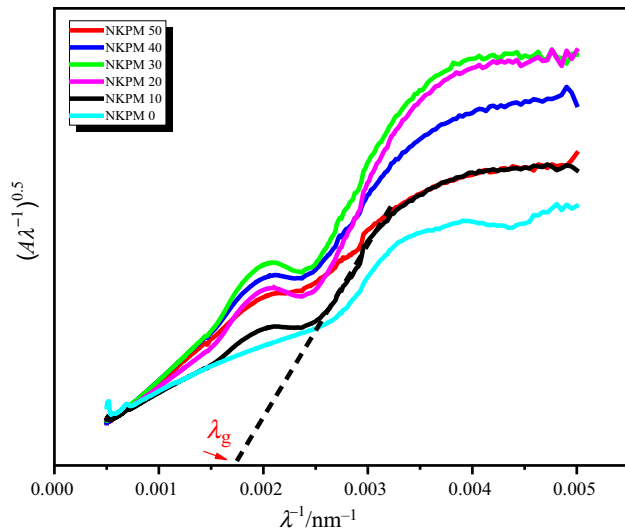
Fig. 9 Variation in $(A\lambda)^{0.5}$ as a function of $(1/\lambda)$ for the studied glasses (ASF method)

Fig. 10 Energy gap values for $(1-x)$ $(0.5NaPO_3–0.5KPO_3)–xMnO_2$ glasses determined by Tauc's and ASF methods as a function of MnO_2 content (line is drawn as a guide to the eye)

Table 3 Optical band gap and Urbach energy of the $(1-x)$ $(0.5NaPO_3–0.5KPO_3)–xMnO_2$ glasses

Sample code	E_g/eV Tauc's method	E_g/eV ASF method	Urbach energy ΔE/eV
NKPM0	2.40	2.42	0.34
NKPM10	2.20	2.33	0.37
NKPM20	1.90	2.21	0.42
NKPM30	1.75	1.85	0.46
NKPM40	1.45	1.44	0.48
NKPM50	1.44	1.40	0.54

content (Fig. 12). It has been suggested that the value of ΔE is attributed to the structural disorder in amorphous solid. The higher this energy is, the higher the disorder or defect degree is. The observed trend is compatible with the increase in the structural disorder of glasses when the amount of MnO_2 increases. Such a disorder increase is linked to the formation of NBO atoms and defects in the glass structure.

EPR spectroscopy

In order to identify the nature of the paramagnetic entities existing in the framework of the glasses, the electron paramagnetic resonance (EPR) measurements were recorded. EPR is one of the interesting methods and a powerful tool for the characterization of the local structure around paramagnetic probes in glasses. The information about this local structure allows us to understand the correlation between the properties and structure. The EPR is selective spectroscopy, and in the case of manganese-based materials, it is
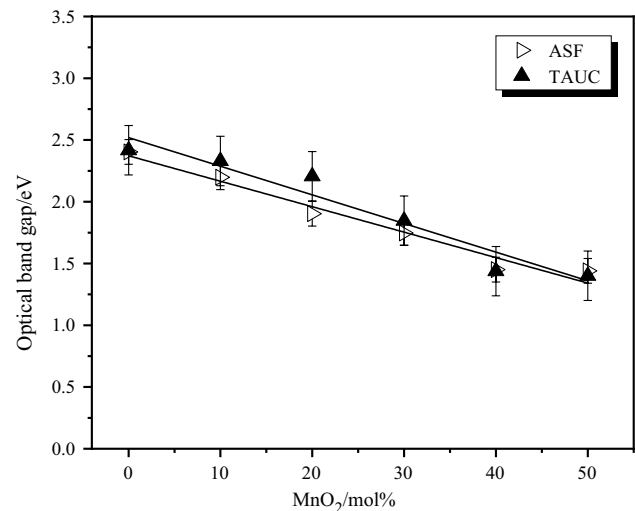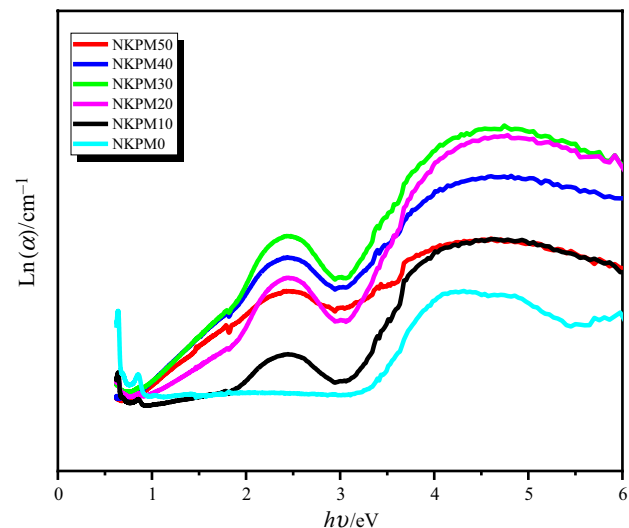

Fig. 11 Variation in $\ln(\alpha)$ as a function of photon energy ($h\upsilon$) for the glasses

only sensitive to Mn^{2+} ions. The EPR spectra of the $(1-x)$ $(0.5NaPO_3–0.5KPO_3)–xMnO_2$ ($0 \leq x \leq 50$ mol%) glasses at room temperature are shown in Fig. 13. As can be seen, the spectra are similar and almost superimposable. They are dominated by a peak centered around $g = 2.02$ (Table 3). Generally, the EPR spectra of Mn^{2+} ($3d^5$) ions in oxide glasses consist of resonance absorption at about $g = 4.3$, 3.3 and 2.0, their relative intensity being strongly dependent on composition [24]. The $g = 4.3$ resonance line is typical for isolated Mn^{2+} ions disposed in cubic symmetric sites lightly tetragonal or rhombically distorted. The $g = 3.3$ resonance
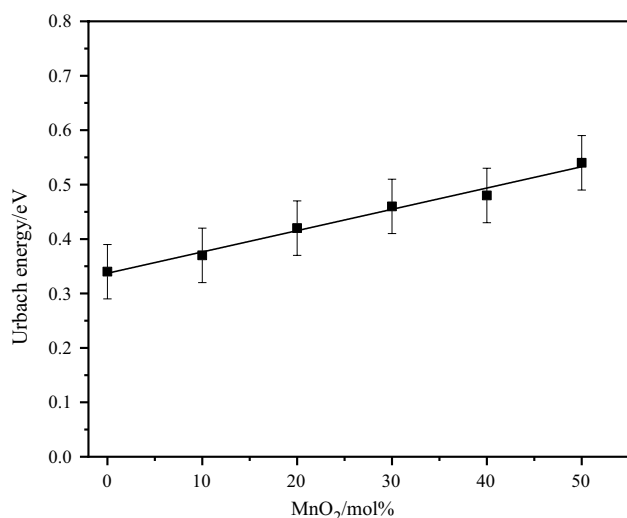
Fig. 12 Composition dependence of the Urbach energy (line is drawn as a guide to the eye)
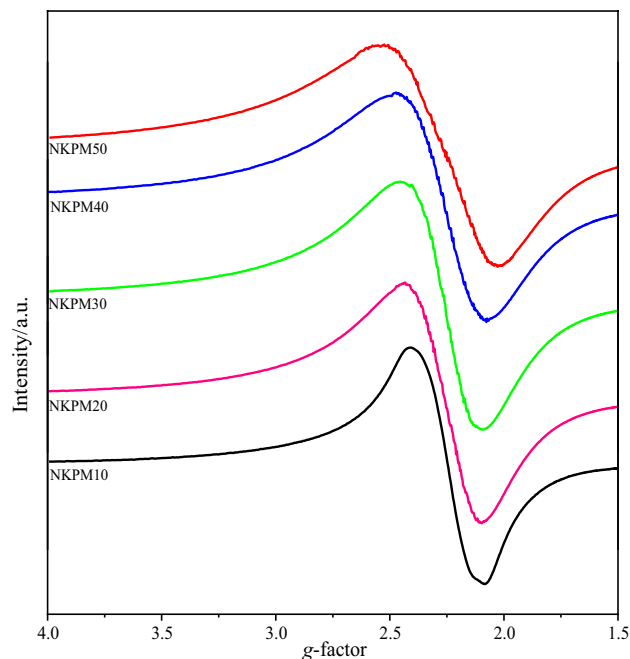

Fig. 13 EPR spectra of the studied glasses

absorption arises from isolated Mn^{2+} ions situated in octahedral sites subjected to strong crystalline field effects [25]. The EPR line around $g = 2.0$ is associated with Mn^{2+} in an octahedral environment with low distortion. From the analysis of Fig. 13, one can deduce that Mn^{2+} in the glasses under study is located in nearly octahedral sites in agreement with the optical results. It is noted that the EPR spectra show no hyperfine structure, suggesting that the Mn^{2+} ions are involved in dipole–dipole type interactions.

Electrical properties

The electrical conductivity of the glasses is determined by the impedance spectroscopy as a function of frequencies at different temperatures. The investigation is undertaken in order to identify the introduction effect of manganese on the transport properties of the glasses. The Mn-free glass NKPM0 ($x = 0$) corresponds to a mixed alkali effect with a minimum in electrical conductivity [10]. Figure 14a shows the Cole–Cole plots of this NKPM0 glass at different temperatures (403, 423 and 443 K). A pseudo-line at low frequency represents the polarization effect in the vicinity of the electrode. This part is the characteristic of the diffusion phenomena and the accumulation of Na$^+$/K$^+$ ions in the electrolyte–electrode interface. A semicircle at high frequency is associated with the bulk response of this glass. The electrical conductivity is calculated by applying the following equation:

$$\sigma = \frac{e}{s}\frac{1}{R} \tag{7}$$

where "e" is the thickness, "s" is the cross-sectional area of the pellet and "R" is the sample resistance at zero frequency.

It is found that the ionic conductivity of this vitreous material is similar to that reported in the literature [10]. However, the actual conductivity is some what higher (Table 5). This difference can be attributed to the synthesis conditions and the thermal history of the samples. The Cole–Cole plots of the Mn-doped glasses are determined. It is found that the electrical conductivity is decreased in manganese doping glasses so that it is not possible to obtain the perfect Nyquist plots for them except for the glass NKPM10 (Fig. 14b). The plots in this later figure show semicircle at high frequency, but the spike at low frequency is disappeared in this Mn-doped glass.

It is well known that the ionic conductivity of the glasses depends on the mobility and the density of the charge carriers. Also, it depends on the pathway followed by the charge carrier ion inside the structure. The decrease in the conductivity with Mn doping in the glasses $(1 - x)$ (NaPO$_3$–KPO$_3$)–xMnO$_2$ could be understood by considering the variation in the charge carrier concentration. As a matter of fact, the charge carriers ions could be Na$^+$, K$^+$, and polarons issued from manganese species. It seems that the content alkali ions play a great role in the electrical transport properties of the glasses since the introduction of manganese at the expense of mobile Na$^+$, K$^+$ diminishes the conductivity of the NKPM10 glass. Moreover, the decrease in the conductivity can be explained by the reticulation effect of manganese in the glasses. In fact, the substitution of Na and K by Mn has induced the reticulation of the network which renders the glass structure more closed, and the mobility of alkali ions could be reduced.
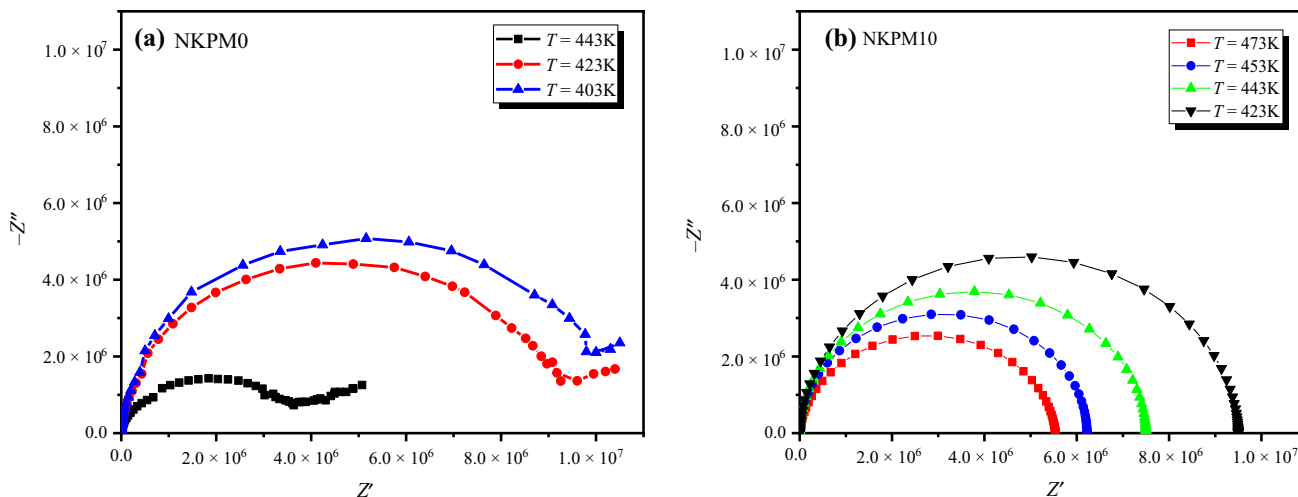
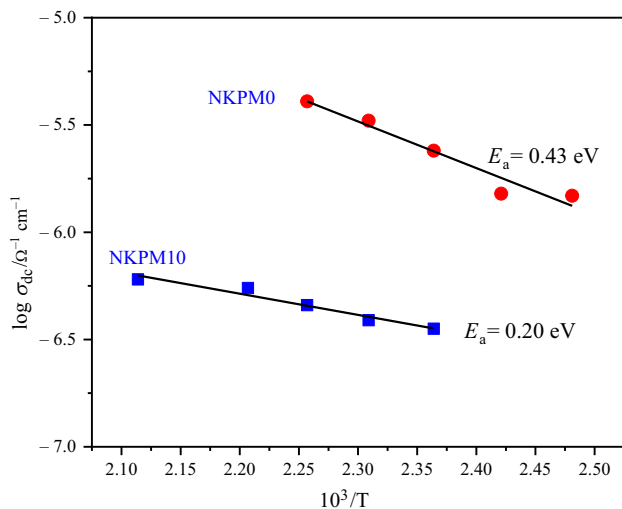**Fig. 14** Cole–Cole plots relative to NKPM0 ($x = 0$) and NKPM10 ($x = 10$)

Fig. 15 log (σ_{dc}) versus 1000/T plots for the NKPM0 and NKPM10 glasses

Table 4 Electrical conductivity and activation energy of NKPM0 and NKPM10 glass samples

Sample	Composition/ mol%	log $\sigma_{dc(423K)}$	E_a/eV
NKPM0	0	−5.79	0.43
NKPM10	10	−6.45	0.20

E_a in the NKPM10 glass. This assumption is in agreement with the absence of spike at low frequency in the Cole–Cole plots of this glass. Furthermore, the electronic conduction in NKPM10 is ascertained by the presence of manganese in + 2 and + 3 oxidation states in the glassy network as suggested by EPR and UV–Vis absorption studies. These Mn^{2+} and Mn^{3+} cations provide the pathway for the exchange of electrons necessary for electronic conduction.

Crystallization of the glasses

The crystallization of the vitreous materials is carried out by heat treatments at the crystallization temperature determined from the DTA curves. This temperature varies from 510 to 600 °C upon the glass composition. Then, the glass–ceramics (GC) are analyzed by XRD in order to identify the formed crystalline phases. Figure 16 shows the obtained XRD patterns for each composition. At lower concentration of manganese oxide (x = 0 and 10 mol%), the XRD patterns of the GC-NKPM0 and GC-NKPM10 are dominated mainly by metaphosphate phases KPO_3 (JCPDS 98-000-6146) and $KNa_2(PO_3)_3$ (JCPDS 98-000-2346). The XRD pattern of the glass–ceramic NKPM20 shows a broad halo, suggesting that this compound is thermally stable in agreement with the DTA data (high T_c–T_g).

The temperature dependence of the conductivity of NKPM0 and NKPM10 is shown in Fig. 15. These variations demonstrate that the conductivity of the glasses is thermally activated and follows an Arrhenius behavior:

$$\sigma \sim \exp\left(-E_a/kT\right) \tag{8}$$

where E_a is the activation energy and "k" the Boltzmann constant.

These electrical parameters are given in Table 4. It is observed that the activation energy of the NKPM10 glass is lower than that of the NKPM0 glass, suggesting that the conduction mechanism is changed by Mn doping. An electronic conduction process could be the origin of the low value of
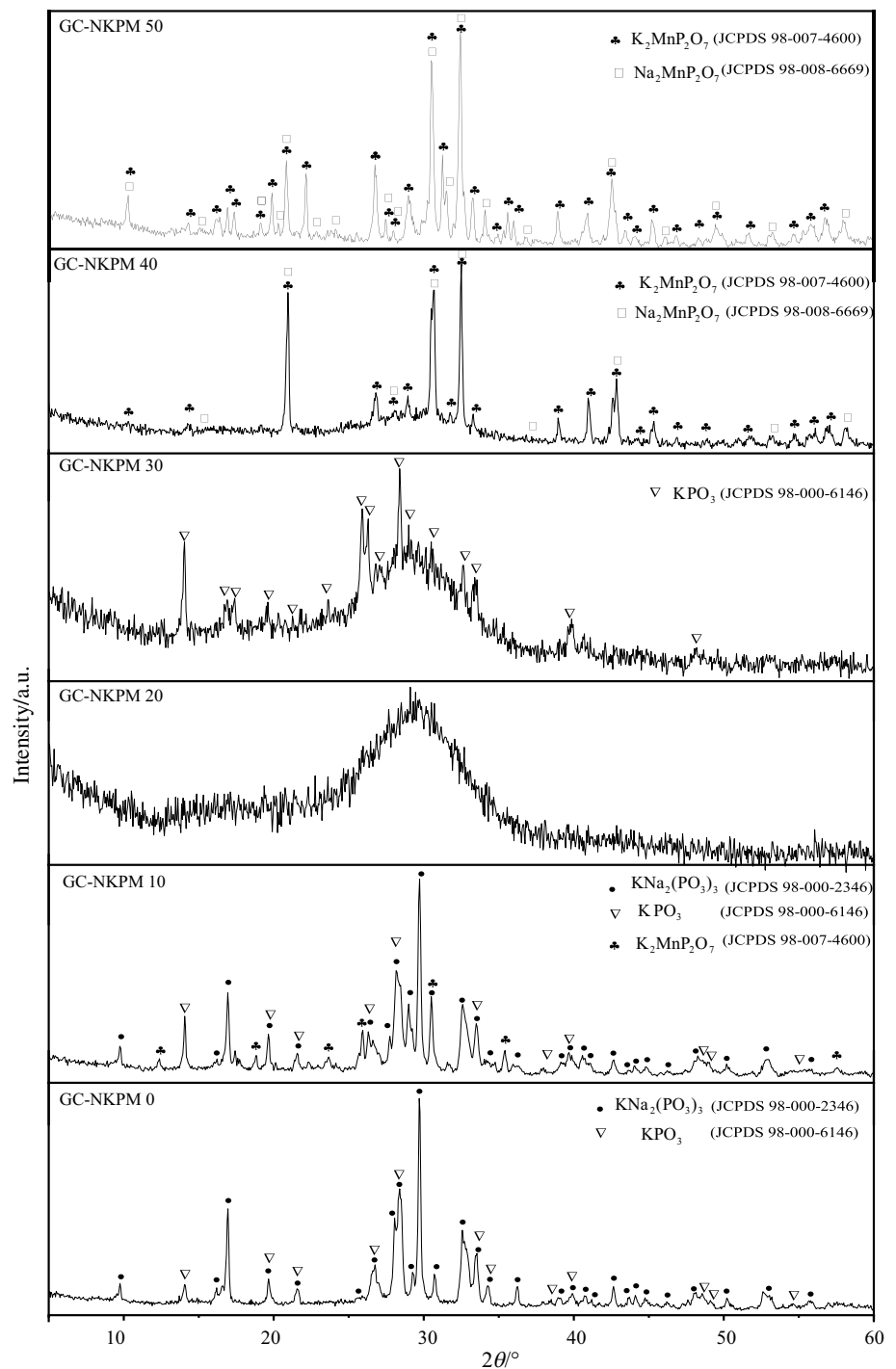
Fig. 16 XRD patterns of the crystallized glasses

When the concentration of manganese increases further to $x = 40$ and 50 mol%, one can note the emergence of two pyrophosphate phases K$_2$MnP$_2$O$_7$ (JCPDS 98-007-4600) and Na$_2$MnP$_2$O$_7$ (JCPDS 98-008-6669). According to the crystallographic data of K$_2$MnP$_2$O$_7$ and Na$_2$MnP$_2$O$_7$ [26], each Mn^{2+} ion is located in the octahedral site (MnO$_6$) surrounded by four P$_2$O$_7$ groups. Therefore, the formation

of these phases is in accordance with the IR analysis of the glasses. The significant IR bands detected at 1098 cm^{-1} and 1020 cm^{-1} are attributed to pyrophosphate structural units, and a band at 622 cm^{-1} is ascribed to MnO$_6$ group. The XRD analysis does indicate that the structural role of manganese oxide is a glass modifier.
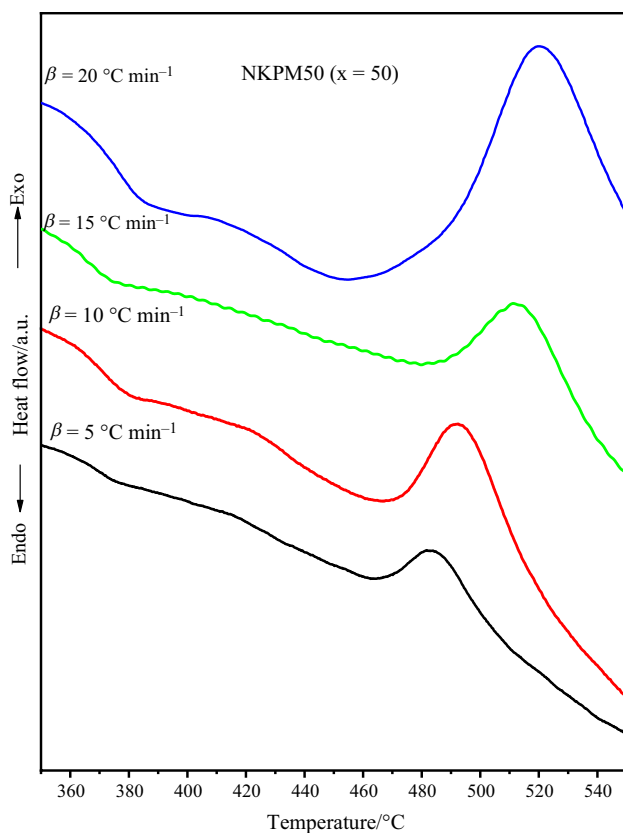
Fig. 17 DTA curves for the NKPM50 under different heating rates

Crystallization kinetic

The kinetic parameters of the glass crystallization such as activation energy (E_c) and Avrami exponent (n) are obtained by monitoring the displacement on the crystallization peak as a function of the heating rate. The energy (E_c) is determined by applying the relationship [27]:

$$\mathrm{Ln}\,(T_c^2/\beta) = E_c/(RT_c) + \text{constant} \tag{9}$$

where β and R are the heating rate and the gas constant, respectively.

The composition NKPM50 ($x = 50$) is selected for the crystallization kinetic study since its DTA curve shows a net crystallization peak. The obtained DTA curves at different heating rates β: 5, 10, 15, 20 °C min^{-1} are presented in Fig. 17. From the analysis of this latter figure, it is seen that the crystallization peak shifted to higher temperatures from 481 to 512 °C with an increased in heating rate. The plot of $\ln(T_c^2/\beta)$ versus the inverse of temperature (Fig. 18) is linear, and the activation energy for crystallization could be determined from the slope of this straight line. The determined value for E_c is 203.75 kJ·mol^{-1}. This energy value depends on the dissociation bond energy
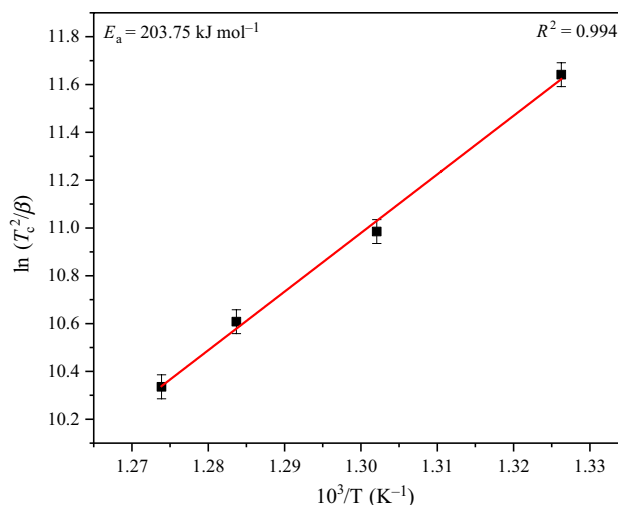

Fig. 18 Plot of ln (T_c^2/β) versus inverse temperature for the NKPM50 glass

of the glassy network. According to ref [28], the energy of the Na–O, K–O, Mn–O and P–O bonds is, respectively, 256.1 kJ mol^{-1}, 277.8 kJ mol^{-1}, 362 kJ mol^{-1} and 589 kJ mol^{-1}. Hence, low energy is needed to break alkali M–O (M=Na, K) links as compared to the others. The substitution of a part of the weak M–O bonds by Mn–O results in the formation of a new modifier site MnO$_6$. In sum, two different modifier sites coexist in the network. While one is occupied by a mixture of alkali (Na/K), the other one is occupied by manganese. It seems that the crystallization of Na$_2$MnP$_2$O$_7$ and K$_2$MnP$_2$O$_7$ in the glass–ceramics is due to the easy break of the alkali sites. In order to shed more light on the crystallization mechanism either bulk or surface, the DTA curves are served as a base to determine the Avrami parameter (n) from the following equation [29]:

$$n = (2.5/\Delta T) \times (RT_c^2 / E_c) \tag{10}$$

where ΔT is the width at the half-height of the crystallization peak and E_c is the activation energy. The value calculated for n varies from 1.03 to 1.57 (Table 5), suggesting that the surface crystallization mechanism is dominant during the crystallization of the glasses under heat treatments.

Table 5 Crystallization temperature and Avrami parameter of the glass NKPM50 ($x = 50$) for different heat crystallization rates

Glass	β/°C min^{-1}	T_c/°C	ΔT/°C	E_c/kJ mol^{-1}	Avrami parameter (n)
NKPM50 ($x = 50$)	5	481	15	203.75	1.57
	10	495	18		1.39
	15	506	24		1.09
	20	512	26		1.03

Conclusions

The most interesting conclusions drawn from the investigation of some physical, spectroscopic and electric properties of the $(1 - x)(0.5NaPO_3–0.5KPO_3)–xMnO_2$ ($x = 0–50$ mol%) glasses are summarized as follows:

(1) The increase in the density and the glass transition temperature with the addition of MnO$_2$ in the base glass $(0.5NaPO_3–0.5KPO_3)$ corroborates the formation of covalent P–O–Mn bonds in the expense of (PO^-, Na^+) and/or (PO^-, K^+) ionic bonds.

(2) The IR spectroscopy shows that some metaphosphate structural units in the glasses are converted to monophosphate groups when the content of MnO$_2$ is higher than 20 mol%.

(3) The optical absorption measurements indicate the presence of both Mn^{2+} and Mn^{3+} ions. The absorption bands relatives to these species are very broad.

(4) The ESR spectra are characterized by a relative signal around $g = 2.02$. This signal is attributed to the Mn^{2+} ions in an environment close to octahedral symmetry.

(5) The Dc conductivity of the glasses is thermally activated and followed an Arrhenius behavior. It decreases with the addition of MnO$_2$ owing to the decrease in the alkali cation concentrations.

(6) The crystallization of the glasses containing manganese induces the formation of pyrophosphate K$_2$MnP$_2$O$_7$ and Na$_2$MnP$_2$O$_7$ phases. The surface crystallization was the dominant mechanism.

It is worth noting the glasses under study exhibit high thermal stability and low melting temperature. Such Phosphate materials could offer suitable properties in order to use them as additives for sintering and consolidation of energy materials.

References

1. Sinouh H, Bih L, Azrour M, El Bouari A, Benmokhtar S, Manoun B, Belhorma B, Baudin T, Berthet P, Haumont R, Solas D. Elaboration and structural characterization of glasses inside the ternary SrO–TiO$_2$–P$_2$O$_5$ system. J Phys Chem Solids. 2012;73:961–8.

2. Bih L, Allali N, Yacoubi A, Nadiri A, Levasseur A. Thermal, physical and spectroscopic investigations of P$_2$O$_5$–A$_2$MoO$_4$–A$_2$O (A = Li, Na) glasses. J Phys Chem Glass. 1999;40:229–34.

3. Rajiv A, Reddy MS, Uchil J, Reddy CN. Photoluminescence studies of NaPO$_3$–ZnO–MnO$_2$ glass system. J Lumin Appl. 2015;5:41–4.

4. Pascuta P, Bosca M, Borodi G, Culea E. Thermal, structural and magnetic properties of some zinc phosphate glasses doped with manganese ions. J Alloys Compd. 2011;509:4314–9.

5. Szumera M, Wacławska I. Thermal study of Mn-containing silicate-phosphate glasses. J Therm Anal Calorim. 2012;108:583–8.

6. Venkateswara Rao NVG, Yadagiri Reddy P. Thermoluminescence studies on Li$_2$O–CaF$_2$–B$_2$O$_3$ glasses doped with manganese ions. J Mater Lett. 2002;57:403–8.

7. Omrani RO, Krimi S, Videau JJ, Khattech I, El Jazouli A, Jemal M. Structural investigations and calorimetric dissolution of manganese phosphate glasses. J Non-Cryst Solids. 2014;389:66–71.

8. Ahmina W, El Moudane M, Zriouil M, Taibi M. Glass-forming region, structure and some properties of potassium manganese phosphate glasses. J Phase Trans. 2016;89:1051–61.

9. Jerroudi M, Bih L, Azrour M, Manoun B, Saadoune I, Lazor P. Investigation of novel low melting phosphate glasses inside the Na$_2$O–K$_2$O–ZnO–P$_2$O$_5$ system. J Inorg Organomet Polym Mater. 2019. https://doi.org/10.1007/s10904-019-01213-0.

10. Tsuchida JE, Ferri FA, Pizani PS, Rodrigues ACM, Kundu S, Schneiderce JF, Zanotto ED. Ionic conductivity and mixed-ion effect in mixed alkali metaphosphate glasses. J Phys Chem. 2017;19:6594–600.

11. Taylor P, Davis EA, Mott NF. "Conduction in non-crystalline systems V. Conductivity, optical absorption, and photoconductivity in amorphous semiconductors. Philos Mag. 2012;22(37–41):2006.

12. Souri D, Tahan ZE. A new method for the determination of optical band gap and the nature of optical transitions in semiconductors. J Appl Phys. 2015;119:273–9.

13. Urbach F. The long-wavelength edge of photographic sensitivity and of the electronic absorption of solids. J Phys Rev. 1953;92:61.

14. Feller SA, Lower N, Affatigato M. Density as a probe of oxide glass structure. J Phys Chem Glass. 2001;42:240–6.

15. Ray NH. Property relationships in inorganic oxide glasses. J Non-Cryst Solids. 1974;15:423–34.

16. El Hezzat M, Et-tabirou M, Montagne L, Bekaert E, Palavit G. Structure and ac conductivity of sodium–lead–cadmium metaphosphate glasses. J Mater Lett. 2003;58:60–6.

17. Khafagy AH. Infrared and ultrasonic investigations of some $[(MnO_2)_x–(P_2O_5)_{100-x}]$ 1 wt% Nd$_2$O$_3$ glasses. J Phys Stat Solids. 2001;114:105–14.

18. Richard K. Review: the structure of simple phosphate glasses. J Non-Cryst Solids. 2000;263:1–28.

19. Pascuta P, Borodi G, Jumate N, Vida-Simiti I, Viorel D, Culea E. The structural role of manganese ions in some zinc phosphate glasses and glass ceramics. J Alloys Compd. 2010;504:479–83.

20. Bae B, Weinberg MC. Ultraviolet optical absorptions of semiconducting copper phosphate glasses. J Appl Phys. 2014;73:7760–6.

21. Winterstein-beckmann A, Möncke D, Palles D, Kamitsos EI, Wondraczek L. Structure–property correlations in highly modified Sr,Mn-borate glasses. J Non-Cryst Solids. 2013;376:165–74.

22. Konidakis I, Varsamis CPE, Kamitsos EI, Möncke D, Ehrt D. Structure and properties of mixed strontium–manganese metaphosphate glasses. J Phys Chem C. 2010;114:9125–38.

23. El Batal FH, Marzouk SY, Nada N, Desouky SA. Optical properties of vanadium-doped bismuth borate glasses before and after gamma-ray irradiation. Philos Mag. 2010;90:675–97.

24. Ramadevudu G, Rao SLS, Chary MN. Physical, optical, and spectroscopic studies on MgO–BaO–B$_2$O$_3$ glasses. London: Hindawi Publishing Corporation; 2013. p. 1–11.

25. Ardelean I, Mureşan N, Păşcuţă P. EPR and magnetic susceptibility studies of manganese ions in 70TeO$_2$–25B$_2$O$_3$–5SrO glass matrix. J Mater Chem Phys. 2007;101:177–81.

26. Gravereau P, et al. Synthesis, crystal structure, and vibrational spectroscopic and UV–visible studies of $Cs_2MnP_2O_7$. J Solid State Chem. 2013;198:379–85.

27. Kissinger HE. Variation of peak temperature with heating rate in differential thermal analysis. J Res Natl Bur Stand. 1956;57:217–21.

28. Lide DR, editor. CRC handbook of chemistry and physics. Boca Raton: CRC Press; 2001.

29. Augis JA, Bennett JE. Calculation of the Avrami parameters. J Therm Anal. 1978;13:284–93.